remote sensing

MDPI

Article

A Time-Domain Doppler Estimation and Waveform Recovery Approach with Iterative and Ensemble Techniques for Bi-Phase Code in Radar Systems

Ahmed Youssef [1,*], Belaid Moa [2] and Peter F. Driessen [2]

[1] Radar Department, Military Technical Collage, Cairo 11588, Egypt
[2] Electrical and Computer Engineering Department, University of Victoria, Victoria, BC V8P 5C2, Canada; bmoa@uvic.ca (B.M.); peter@ece.uvic.ca (P.F.D.)
* Correspondence: afyousef@mtc.edu.eg

Abstract: This paper presents a novel, cost-effective technique for estimating the Doppler effect in the time domain using a single pulse and subsequently leveraging the precise Doppler value to recover the radar waveform. The proposed system offers several key advantages over existing techniques, including the ability to calculate the target speed without any frequency ambiguity and the ability to detect a wide range of target speeds. These two features are not available in any existing techniques, including the conventional moving target detection (MTD) processor. To ensure improved accuracy and robust estimation, the system employs ensemble and iterative techniques by recursively and efficiently reducing the Doppler residues from the signal. Furthermore, the proposed system demonstrates effective signal recovery of a well-known bi-phase code shape at low signal-to-noise ratios in just a few iterations. The performance evaluation of the new algorithm demonstrates its practicability and its superiority over traditional radar systems. Implementation on software-defined radio (SDR) reveals that the proposed system excels in Doppler estimation and signal recovery at low SNRs, demonstrating promising results.

Keywords: radar systems; Doppler estimation; signal recovery; bi-phase signal; signal-to-noise ratio; software-defined radar

check for updates

Citation: Youssef, A.; Moa, B.; Driessen, P.F. A Time-Domain Doppler Estimation and Waveform Recovery Approach with Iterative and Ensemble Techniques for Bi-Phase Code in Radar Systems. *Remote Sens.* **2024**, *16*, 2300. https://doi.org/10.3390/rs16132300

Academic Editor: Stefano Tebaldini

Received: 9 April 2024
Revised: 16 June 2024
Accepted: 20 June 2024
Published: 24 June 2024

Copyright: © 2024 by the authors. Licensee MDPI, Basel, Switzerland. This article is an open access article distributed under the terms and conditions of the Creative Commons Attribution (CC BY) license (https://creativecommons.org/licenses/by/4.0/).

1. Introduction

Many radar systems use frequency- or phase-modulated signals as their typical waveforms. Each modulated waveform enjoys its own advantages, along with its disadvantages [1,2]. A linear frequency modulation (LFM) and bi-phase-coded signal are good examples of classical radar waveforms. On one hand, LFM has a high Doppler tolerance feature and high compression ratio, but it suffers from time-sidelobe effects. On the other hand, bi-phase-coded signals are known for their low sidelobes, but they have a Doppler-intolerant waveform with a limited compression ratio [3–5].

The Doppler effect is a critical aspect of radar measurements, as it hinders the effectiveness of radar signals [6–8]. Moreover, especially in the case of high-speed targets, it may distort the signal phase and, therefore, no target information would be extracted. This happens for most bi-phase codes, including Barker codes. If we are able to eliminate or even suppress the Doppler effect, we can improve the quality of the range resolution of phase-coded radar signals.

We believe that our paper is the first to discuss both time-domain Doppler estimation and the signal recovery of bi-phase modulation signals in a radar background. In fact, we performed a thorough literature review, carefully examining existing research, from the oldest to the most recent, to ensure that we did not miss any relevant research in this area.

In [9], the authors proposed a decision-directed Doppler estimation method based on the frequency average for phase-shift keying (PSK) signals for underwater acoustic communications. This estimation is achieved by averaging the frequency estimates from a bank of correlators. A robust estimate can be further computed by increasing the observation intervals at the expense of the computational cost. This method, however, is limited to underwater targets with very slow speeds.

Doppler estimation is achieved in [10] using the dual alternating-direction method (ADM) with standard statistical tools and a multiple-hypothesis testing procedure using a few pulses and without any frequency or phase modulation. Although the method introduced a good range and Doppler estimation, it gave only approximate values due to cell accuracy. In [11], the authors attempted to estimate the real-time Doppler effect using up–down and up–mute–down hyperbolic frequency modulation methods. The estimation is based on finding the relationship between the Doppler scaling factor (the rate of change in the delay of a signal in a time-varying channel) and the time delay of the signal at the receiver. Unfortunately, the method was found inadequate for low-speed targets.

The authors of [12] managed to compensate for the Doppler effect on complementary phase modulation signals. By creating a new complementary code of length N and multiplying each sample at index n by the conjugate of the adjacent sample at $n + 1$ in the new code, the method is able to produce the desired compensated code. Although this approach is straightforward for short codes, it becomes increasingly complex and computationally intensive as the code length increases. Additionally, this method was only tested on targets moving at moderate speeds. Furthermore, after compensation, the Doppler information is lost, preventing the determination of the target velocity.

Another method for Doppler estimation was proposed in [13], and it relied on a combination of hyperbolic frequency modulation and speed spectrum scanning. Although the method reduces interference in speed spectrum peak detection and improves the accuracy of the estimation, the success of this method requires high sampling rates. In addition, the signal suffers from high time sidelobes, which can affect nearby targets.

Yet another Doppler estimation method can be found in [14], and it was primarily developed for non-terrestrial networks. The method involves using reference signals at different frequency positions in an OFDM carrier to estimate the Doppler shift for high-speed targets. Using this method, a system can calculate the required frequency adjustment value and use it to pre-compensate uplink transmissions and to maintain multi-access orthogonality at the receiver. Unfortunately, the range of the errors in the estimated Doppler shifts is between -1.5 kHz and 1.5 kHz, which is not acceptable in many radar applications. Moreover, it is not adequate for radar systems that use a single carrier frequency. In [15], a Doppler cancellation module that integrates data from multiple signals to eliminate Doppler effects from Doppler-intolerant signals, such as phase-modulated signals, is introduced. This allows the use of high-resolution waveforms to detect high-speed targets, even if they are Doppler-intolerant. However, this method does not provide Doppler value estimation and dictates that one of the integrated signals is used for Doppler estimation.

In [16], the authors presented an enhanced orthogonal matching pursuit (OMP) algorithm to directly estimate the velocity and the acceleration of the target. They rely on pre-constructing a dictionary for sparse motion parameters of the target. This renders the Doppler frequency migration unnecessary. While effective for estimating the velocity and the acceleration, this method is iterative, relies on the greedy nature of OMP, and can be very expensive, especially for large dictionaries of the parameter space.

The authors of [17] presented another method for recovering radar waveforms and estimating Doppler values for high-speed targets using two types of waveforms: phase-modulated and unmodulated waveforms. This technique is primarily effective for high-speed targets. For low-speed targets, the authors recommend using traditional Doppler estimation methods, thereby incorporating the proposed method as a sub-module within a typical radar system. Doppler values are estimated using the FFT of the unmodulated

signal. Consequently, the Doppler ambiguity is constrained by the repetition time and the resolution of FFT.

It is worth highlighting that, to estimate the Doppler frequency, most of the methods mentioned above rely on DFT, which makes them unable to resolve the exact Doppler frequency due to DFT's inherent Doppler ambiguity. Moreover, many of the available techniques for estimating Doppler frequency are not suitable for bi-phase signals.

In this paper, we present an efficient and inexpensive algorithm that accurately estimates the Doppler value by relying on just one pulse. The algorithm enhances the robustness of its estimate by using an ensemble averaging of Doppler estimators based on the next few successive pulses. To increase the accuracy even further, we rely on an iterative technique to progressively remove any Doppler residue. Since the estimation is performed in the time domain, the proposed algorithm is immune to all Doppler ambiguities. Thereby, the Doppler ambiguity that occurs in the conventional Doppler calculations does not affect our algorithm. Furthermore, the proposed algorithm segregates the Doppler effect from the signal, removes the Doppler effect from any bi-phased waveform using a sequence of subsystems, and enables the return of the waveform to its well-known shape at low signal-to-noise-ratios (SNRs) to produce a reliable range resolution. By doing so, we decrease the time and hardware complexities from which the conventional radar systems suffer, as they rely on expensive MTD processors with a large coherent pulse interval (CPI). In addition, we circumvent the main bottleneck problem in using bi-phase codes for moving target detection, especially for high-speed targets.

Figure 1 shows a block diagram of our proposed modules in a conventional radar system.

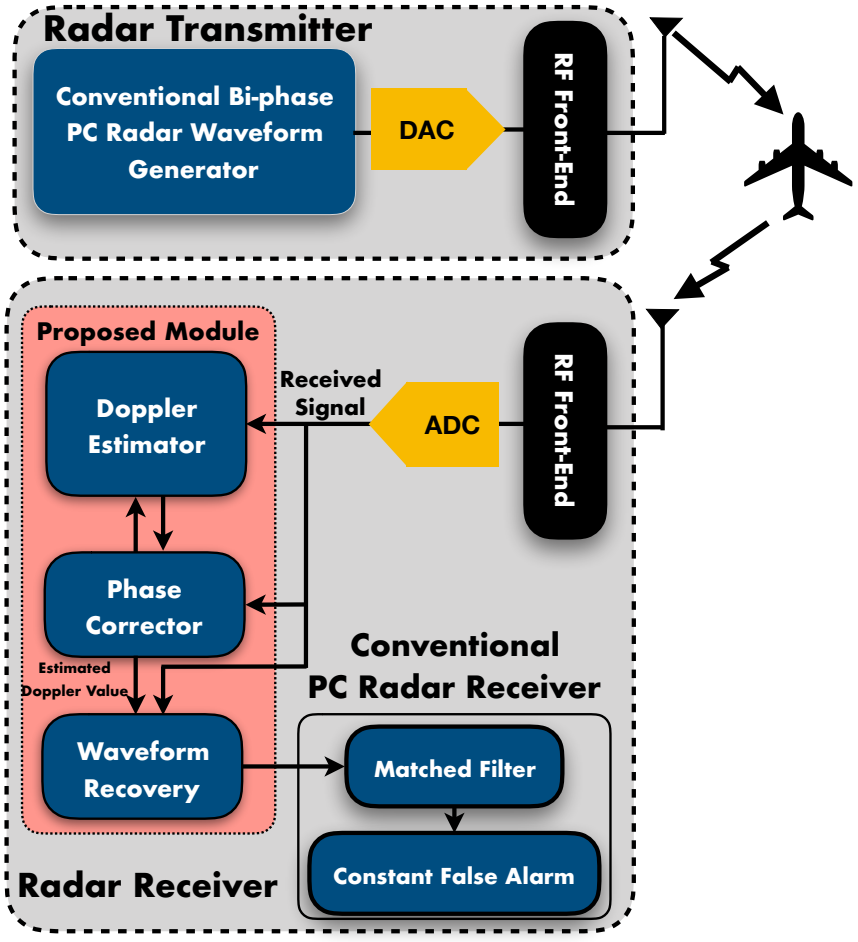


Figure 1. A brief block diagram of our proposed radar system.

As the block diagram depicts, the proposed module can be viewed as an add-on component that sits between the ADC and the rest of the conventional radar receiver modules. Instead of feeding the received signal directly to the matched filter (MF), we first feed it to a sequence of three subsystems (Doppler estimator, phase corrector, and waveform recovery) that form our proposed add-on module. The Doppler estimator applies a nonlinear transformation to the received signal to remove the bi-phase waveform and calculate an estimate for the Doppler value. The phase corrector uses this estimate to reduce the Doppler effect from the received signal and then check if any remainder of the Doppler effect needs to be suppressed. If that is the case, the adjusted signal from the phase corrector is re-fed to the Doppler estimator for further processing. This treatment is repeated until an accurate estimate of the Doppler is obtained. The waveform recovery subsystem uses the boosted estimates of the Doppler value along with the received signal to detect the target speed and recover the original waveform with a minimal Doppler effect. The recovered waveform is then fed to the conventional range radar detector.

It is worth mentioning that the proposed module does not affect the transmitter and is powerful enough to enable the designer to optionally disregard MTD, which requires many pulses to obtain an accurate Doppler estimate without resolving the Doppler ambiguity.

This paper is structured as follows: in Section 2, the algorithm is described analytically, providing an overview of its key components. The simulation results of the proposed algorithm are presented in Section 3, highlighting its performance in a simulated environment. Section 4 investigates the performance of the system and analyzes its effectiveness in practical scenarios. The validation of the theoretical model and the implementation of the algorithm using software-defined radio (SDR) are discussed in Section 5. Furthermore, Section 6 identifies the limitations of the current algorithm and offers potential solutions to overcome them. Finally, in Section 7, the paper concludes by summarizing the key findings and discussing future work that can be pursued in the radar field.

2. Analytical Description of the Proposed Algorithm

In this section, the theory of the proposed algorithm is introduced. A block diagram of the proposed module is shown in Figure 2 and is used to illustrate the main stages of our algorithm.

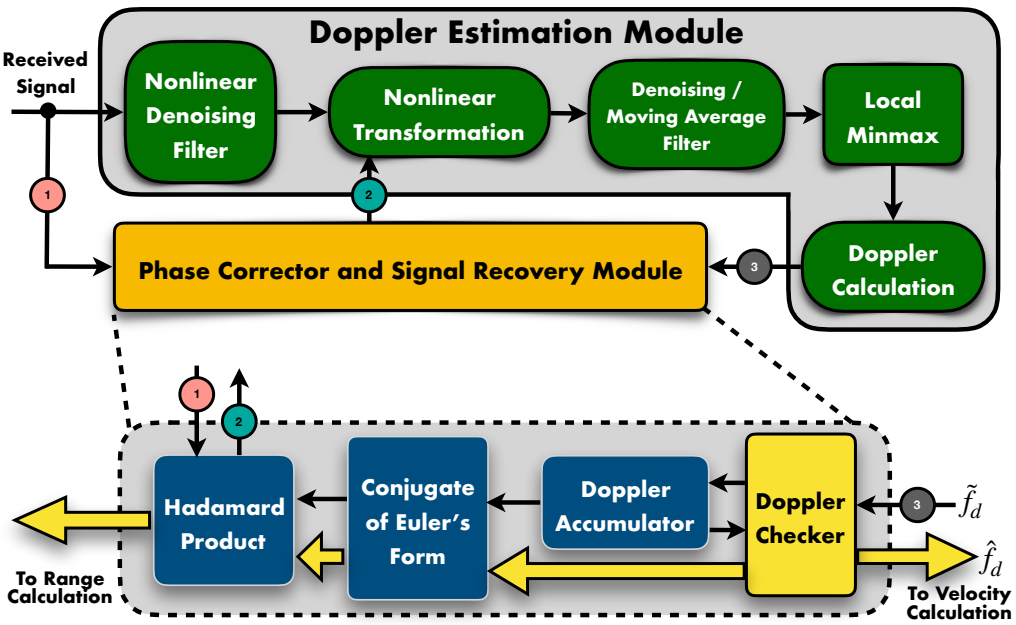


Figure 2. A detailed diagram of the proposed module.

First, we generate a complex baseband bi-phase signal and denote it by $X(t)$. The bi-phase signal is then sent through the traditional modules of a radar transmitter. At the receiver side and after demodulation, the return signal has the following form:

$$R_1(t) = X(t-\tau)e^{-j2\pi f_d(t-\tau)} + n(t), \tag{1}$$

where τ is the target delay, f_d is the target Doppler effect, $n(t)$ is the noise, and $X(t-\tau)$ is the delayed bi-phase waveform. As a pre-processing step, the proposed module uses median filtering, a nonlinear digital filtering technique, to reduce noise and improve the performance of the subsequent processing. This filter is used as it effectively preserves edges during the denoising process [18,19]. With an appropriate window size, the effect of this filter on the signal and noise can be assumed to have the following form:

$$R_2(t) = a_1 X(t-\tau)e^{-j2\pi f_d(t-\tau)} + a_2 n(t), \tag{2}$$

where a_1 and a_2 are real numbers with $a_1 \gg a_2$. The filtered signal is then subjected to a nonlinear transformation $\mathcal{F}$, which enables us to eliminate the effect of the bi-phase and isolate the Doppler effect in the time domain. Although nonlinear transformations were also used in [20], it was primarily to compensate for very low-frequency offsets. In our case, we apply it for the blind estimation of larger Doppler shifts, starting with a coarse estimate, which is then refined in subsequent iterations. Given that we use a bi-phase waveform, we choose $\mathcal{F}$ to be an even power function, in particular, a quadratic one, which we apply in all subsequent iterations of the algorithm.

To illustrate the effect of the transformation, we choose $\mathcal{F}$ to be a quadratic function and apply it to $R_2(t)$, as shown below.

$$\begin{aligned}\mathcal{F}\big(R_2(t)\big) &= R_2(t)^2 \\ &= a_1^2 e^{-j4\pi f_d(t-\tau)} + a_2^2 n^2(t) + 2a_1 a_2 X(t-\tau)n(t)e^{-2\pi j f_d(t-\tau)} \\ &= a_1^2\big(e^{-j4\pi f_d(t-\tau)} + \epsilon^2 n^2(t) + 2\epsilon X(t-\tau)n(t)e^{-2\pi j f_d(t-\tau)}\big),\end{aligned} \tag{3}$$

where $\epsilon = \frac{a_2}{a_1}$. From this equation, we can see that the nonlinear transformation $\mathcal{F}$ serves two objectives: (1) it cancels the bi-phase waveform from the signal, as the term $X(t-\tau)$ represents the bi-phase waveform, which oscillates between $+1$ and -1 depending on its phase. When we apply the nonlinear transformation, the term $X(t-\tau)^2$ always results in 1, cancelling the bi-phase signal, and (2) it turns the multiplicative nature of the Doppler effect into an additive form. In other words, at the receiver, the received signal consists of the delayed signal multiplied by the Doppler effect, in addition to the noise. After transformation, the signal can be represented by three terms, as Equation (3) shows. The first term corresponds to the scaled Doppler signal, the second term represents the pure scaled noise effect, and the last term accounts for the scaled signal multiplied by both noise and the Doppler effect. Given that $\epsilon = \frac{a_2}{a_1} \ll 1$, after filtering and transformation, the effect of the last two terms is reduced by ϵ and can be neglected. This shows the importance of introducing a filter before applying the nonlinear transformation. By combining the last two terms and carrying out a few manipulations, the effect of the nonlinear transformation can also be written as

$$\begin{aligned}\mathcal{F}\big(R_2(t)\big) &= a_1^2 e^{-j4\pi f_d(t-\tau)} + a_2^2 n^2(t) + 2a_1 a_2 X(t-\tau)n(t)e^{-2\pi j f_d(t-\tau)} \\ &= a_1^2 e^{-j4\pi f_d(t-\tau)} + a_2 n(t)\big(2R_2(t) - a_2 n(t)\big) \\ &= a_1^2 e^{-j4\pi f_d(t-\tau)} + N(t).\end{aligned} \tag{4}$$

Therefore, the signal is effectively converted from a Doppler multiplicative form into a pure Doppler additive form. This simplifies our task of extracting Doppler information from the return signal. Although the second term, $N(t)$, has been reduced at the output of the nonlinear denoising filter, we still apply a smoothing filter (to be precise, a moving average

filter) before the Doppler estimator to mitigate the effect of the nonlinear transformation process on the undesirable term, $N(t)$, while reducing the number of noisy, close-by peaks in the first term.

After the smooth filtering, the transformed signal can be considered to have the following form:

$$R(t) = a_3 a_1^2 e^{-j4\pi f_d(t-\tau)} + a_4 N(t), \tag{5}$$

where a_3 and a_4 are $\in \mathbb{R}$ with $a_3 \gg a_4$. The signal is now primed for Doppler estimation and bi-phase signal recovery, as we discuss next.

2.1. Doppler Estimation

The estimation of the Doppler value starts with the local minmax block (see Figure 2). The local minmax algorithm detects the locations of the minima and maxima and assigns them to the arrays l_m and L_M, respectively. This is expressed as follows:

$$\begin{aligned} l_m &= \text{argminima } R(t), \\ L_M &= \text{argmaxima } R(t). \end{aligned} \tag{6}$$

Let us denote by P_m and P_M the sizes of l_m and L_M, respectively. The quantities P_m and P_M derived from the minmax algorithm reflect the density of local minima and maxima in the signal. As the target velocity increases, the frequency modulation induced by the Doppler effect results in a higher density of waveform changes. Consequently, the algorithm detects more minima and maxima within a given time interval, leading to an increase in the size of the l_m and l_M arrays. Three cases present themselves.

Case (1): $P_m \geq 1$ and $P_M \geq 1$. This case can be divided into four sub-cases: $P_M > 1$ and $P_m = 1$, $P_M = 1$ and $P_m > 1$, $P_M = 1$ and $P_m = 1$, and $P_M > 1$ and $P_m > 1$. For the first three sub-cases, the Doppler frequency is calculated as follows:

$$\hat{f_d}^1 = \frac{1}{2n|L_M(1) - l_m(1)|}, \tag{7}$$

where n is the power exponent of the nonlinear transformation, and $\hat{f_d}^1$ is the estimated Doppler effect from the first incoming pulse. If the indices are used, the expression becomes

$$\hat{f_d}^1 = \frac{f_s}{2n|\text{idx}_M(1) - \text{idx}_m(1)|}, \tag{8}$$

where f_s is the sampling frequency, and idx_m and idx_M are the sampling indices of the elements in the arrays l_m and L_M, respectively.

An interesting sub-case is when both P_m and P_M are strictly greater than 1. In this case, we can improve the accuracy of our estimated value based on the ensemble of the estimates as follows:

$$\hat{f_d}^p = \frac{f_s}{2np} \sum_{i=1}^{p} \frac{1}{|\text{idx}_M(i) - \text{idx}_m(i)|}, \tag{9}$$

where $p = \min\{P_m, P_M\}$.

Case (2): $P_m = 1$ and $P_M = 0$, or $P_m = 0$ and $P_M = 1$. Since we only have a single minmax location, we apply the nonlinear transformation again to increase the number of minmax locations and then apply the above case using Equation (9). In this case, the estimate becomes

$$\hat{f_d}^p = \frac{f_s}{2n^2 p} \sum_{i=1}^{p} \frac{1}{|\text{idx}_M(i) - \text{idx}_m(i)|}, \tag{10}$$

Case (3): $P_m = 0$ and $P_M = 0$. This indicates either that the original signal has a very low Doppler value and the algorithm should directly feed it to the MF or that the Doppler

residue is so small that we can terminate the iterations and proceed to signal recovery before the range calculation. In this case, the Doppler estimate is set to 0.

All of the above cases rely on a single pulse. To increase the accuracy of the estimate, an ensemble average can be taken over a few successive pulses as follows:

$$\hat{f}_d{}^p = \frac{1}{N}\sum_{i=1}^{N} \hat{f}_d{}^i, \tag{11}$$

where N is the number of pulses used, and $\hat{f}_d{}^i$ is the Doppler estimate for the ith pulse according to the formulas in the cases above.

2.2. Doppler Checker, Phase Corrector, and Bi-Phase Signal Recovery

In each iteration, the estimated Doppler value, $\hat{f}_d$, is passed to the Doppler checker to decide whether to continue the iterations or proceed to range and velocity calculations, as shown in Figure 2. If $\hat{f}_d \neq 0$, the Doppler checker passes $\hat{f}_d$ to the accumulator, which aggregates the Doppler estimates from the previous iterations.

Since the Doppler estimate can exceed the actual value, the aggregation is not always obvious. In fact, the Doppler checker has to be novel enough to compute the proper sign of $\hat{f}_d$ before passing the signed $\hat{f}_d$ to the accumulator.

The accumulated Doppler value $\tilde{f}_d = \sum \hat{f}_d$ is delivered to the conjugate of the Euler form and Hadamard product blocks to remove the estimated Doppler effect from the signal. Mathematically, the conjugate of the Euler form block computes $e^{2\pi j\tilde{f}_d t}$, while the Hadamard product, an element-wise multiplication between two signals, outputs the following:

$$B(t) = R_1(t)e^{2\pi j\tilde{f}_d t} = e^{j\phi}X(t-\tau)e^{-2\pi j(f_d-\tilde{f}_d)t} + n(t)e^{2\pi j\tilde{f}_d t}, \tag{12}$$

where $\phi = 2\pi f_d \tau$ is the phase effect of the target Doppler delay. Note that $e^{j\phi}$ is a constant, as the Doppler effect and range of targets are unchanged from scan to scan. Therefore, this phase does not affect the local minmax detection.

If $\hat{f}_d$ is 0, the Doppler checker knows that the current Doppler residue is small enough to terminate the iterations and deliver the signal for range and velocity calculations, as shown in Figure 2 with yellow arrows. The ultimate effect of each iteration is, therefore, to reduce the overall Doppler effect f_d by an amount equal to the accumulated Doppler values $\tilde{f}_d$.

Interestingly enough, the expression of $B(t)$ in Equation (12) is analogous to that of $R_1(t)$ in Equation (2) but with a reduced Doppler effect. Therefore, we can recursively repeat the same processing that we used for $R_1(t)$ on $B(t)$ until we obtain a Doppler estimate value $\hat{f}_d \approx 0$.

3. Simulation Results of the Proposed Algorithm

In our simulations, we use the parameters shown in Table 1. The inner workings of the different modules depicted in Figure 1 are detailed in the flowchart presented in Figure 3. On the receiver side, the incoming signal is down-converted by the RF front-end and then digitized by the ADC. A median filter is then applied to the digitized signal. Figure 4a depicts a single-pulse Barker-13 with a coherent pulse interval (CPI) at an SNR of -5 dB. After applying the median filter, we obtain the signal shown in Figure 4b. The figure illustrates the effectiveness of the median filter and its ability to significantly decrease the noise while preserving the edges, including the sharp ones at the points where the signal undergoes a phase flip of π. Performing this step is critical for both achieving accurate estimates of the Doppler frequency and minimizing the number of required iterations.

Table 1. Simulation parameters.

General Radar Parameters	Symbol	Value	Units
Pulse Width	δ	1.3	ms
Pulse Repetition Interval	T_r	3.5	ms
Coherent Pulse Interval	CPI	10	Scalar
Swerlling case		Swerlling II	
Band		L, S, and C Bands	
Selected Carrier Frequency	f_c	4	GHz
Bi-Phase Radar Parameters	**Symbol**	**Value**	**Units**
Sampling frequency	f_s	120	MHz
Bi-phase type		Barker-13	
Target Parameters	**Symbol**	**Value**	**Units**
Target range	τ	30	km
Target Doppler	f_d	0–15	kHz
CFAR type		Order-Statistics CFAR	
CFAR window size	W	8	Range cells
Probability of false alarms	P_{fa}	10^{-6}	-
Noise Parameters	**Symbol**	**Value**	**Units**
Noise type	Additive White Gaussian Noise (AWGN)		

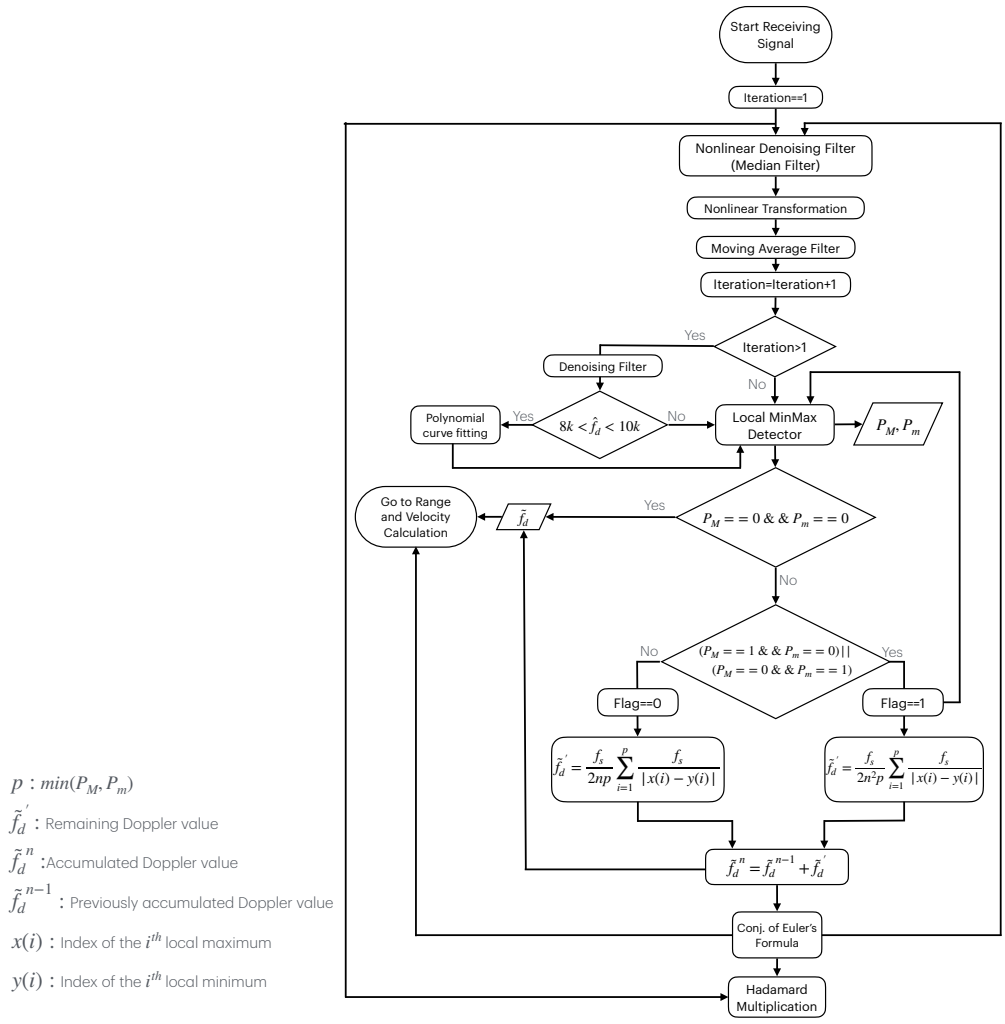


Figure 3. A flowchart of the proposed module.

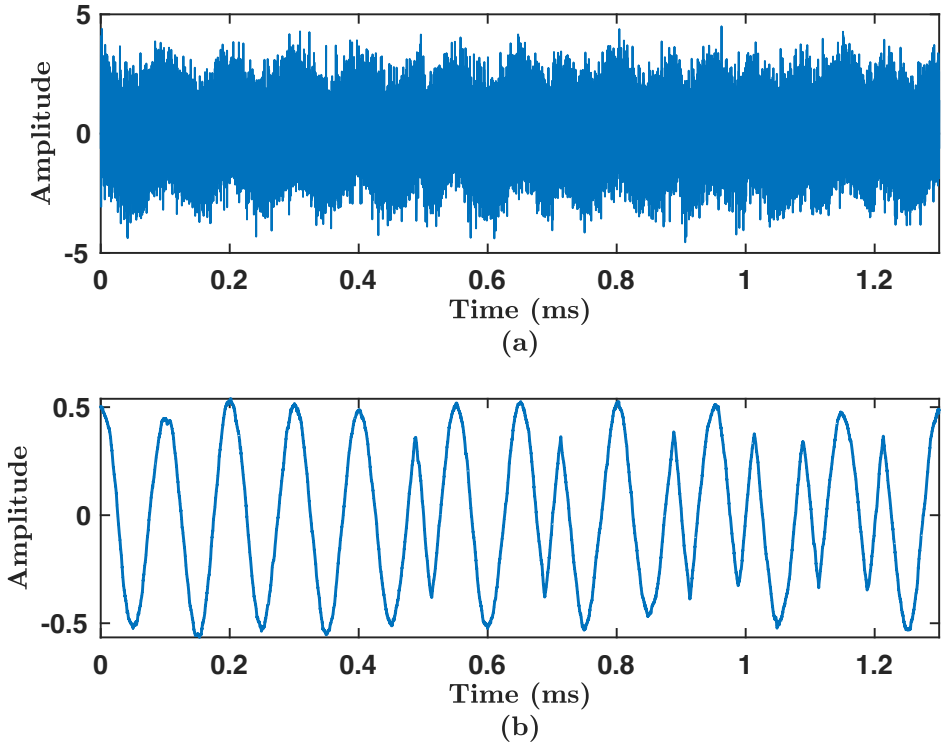


Figure 4. Representation of a single pulse of the received signal at SNR = −5 dB (**a**) before filtering. (**b**) Output of the median filter for a single pulse.

In the first iteration, a nonlinear transformation is applied to the filtered waveform. In our algorithm, we chose a quadratic function to remove bi-phase modulation from the signal and to increase the Doppler cycles. The output from this stage is shown in Figure 5. It is worth pointing out that although the median filter was effective in reducing noise and preserving edges, it was not able to maintain sharp transitions in the bi-phase waveform. This was due to the nature of the median filter, which approximated sharp transitions differently. This, in turn, caused distortions in the Euler form at the output of the nonlinear transformation. The effect of these distortions was minor, as the Doppler estimator relied on ensemble averaging in most cases.

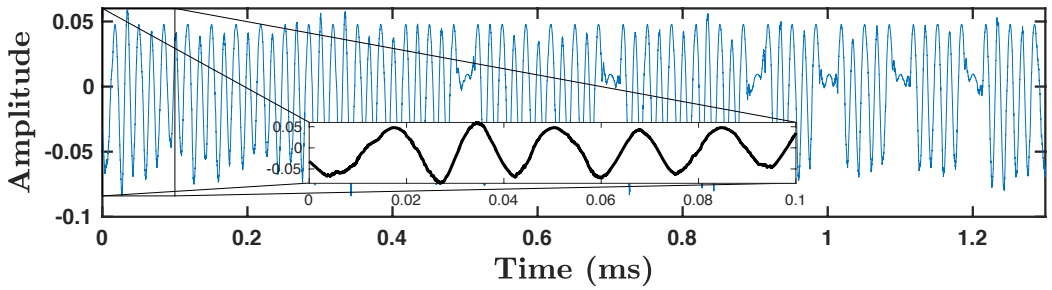


Figure 5. The output of the nonlinear transformation x^2. To improve the clarity, the first 0.1 ms segment of the signal has been enlarged.

A moving average filter was employed before the local minmax detector to increase its robustness by smoothing the noisy, close-by peaks, as shown in Figure 6. While it may appear that the MA filter does not make a substantial difference, it is important to note that before applying the moving average in Figure 5, the signal exhibits noticeable oscillations. If these are mistakenly considered as peaks by the proposed system, it would significantly affect the Doppler estimation. Therefore, the function of the moving average is to smooth these oscillations and ensure a more accurate Doppler estimation.

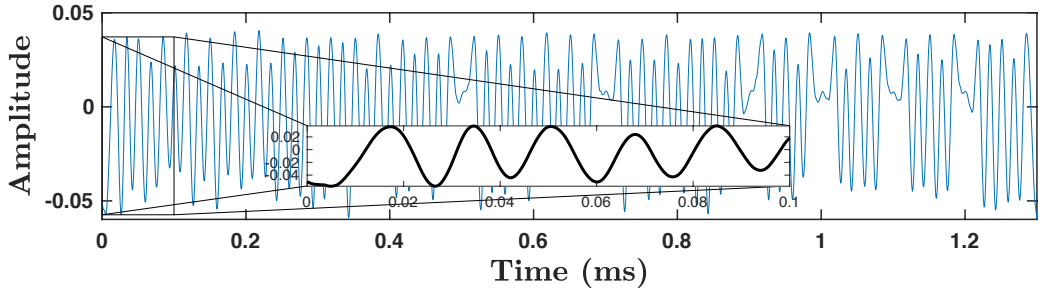


Figure 6. The output of the moving average filter. To improve the clarity, the first 0.1 ms segment of the signal has been enlarged.

The local minmax detector is analogous to the traditional peak-finding algorithm but is also able to detect valleys. The indices from the local minmax detector are then used for Doppler estimation and phase correction, as discussed in Sections 2.1 and 2.2.

Figure 7 shows the signal $B(t)$ obtained from the Hadamard block in the first iteration. By using Equation (12), Figure 7 illustrates how the signal undergoes modulation by both fast and slow signals, which is, of course, caused by the Doppler effect. According to the second term in Equation (12), the noise is modulated by a fast signal due to the estimated Doppler value. This value is very large, as our algorithm was able to accurately approximate the actual Doppler value just from the first iteration. The enlarged portion of the image over a 0.01 ms time interval shows the modulated noise. The median filter used in the proposed algorithm can effectively remove this kind of noise, as illustrated by the red curve in the figure.

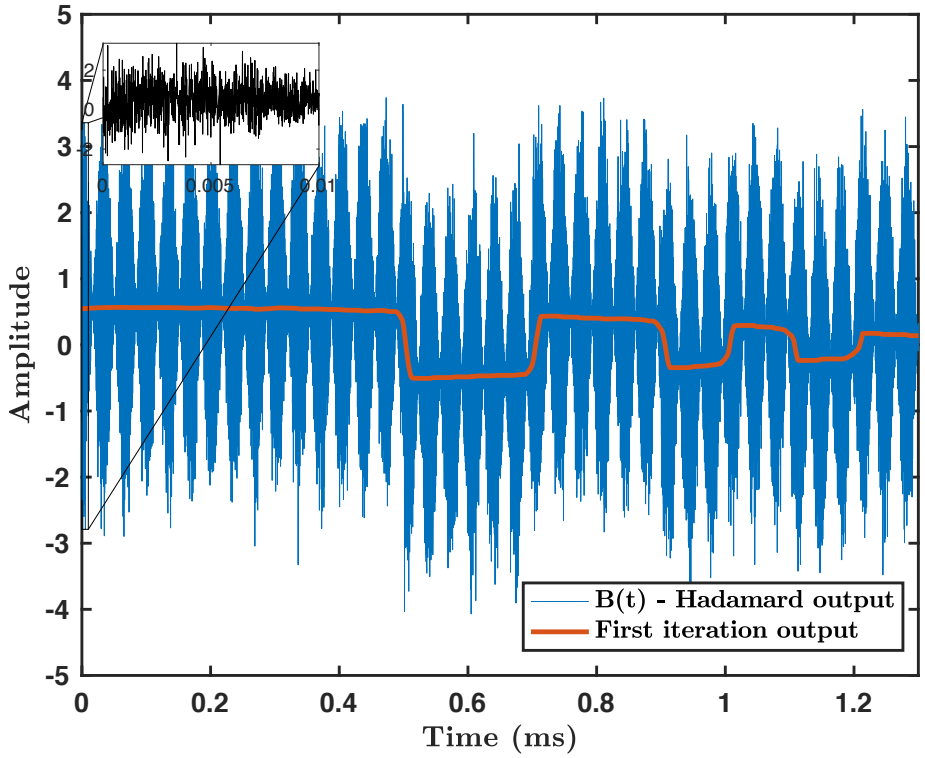


Figure 7. Output of the first iteration. The first 0.01 ms segment of the signal has been enlarged.

The figure also shows a second slow modulation associated with the first term in Equation (12). This slow modulation was due to the Doppler residue after removing the estimated Doppler effect. After filtration, the resulting signal still retains the residual Doppler value, as shown in the same figure using a red color. To show the effect of the second iteration, this signal is also plotted in Figure 8a.

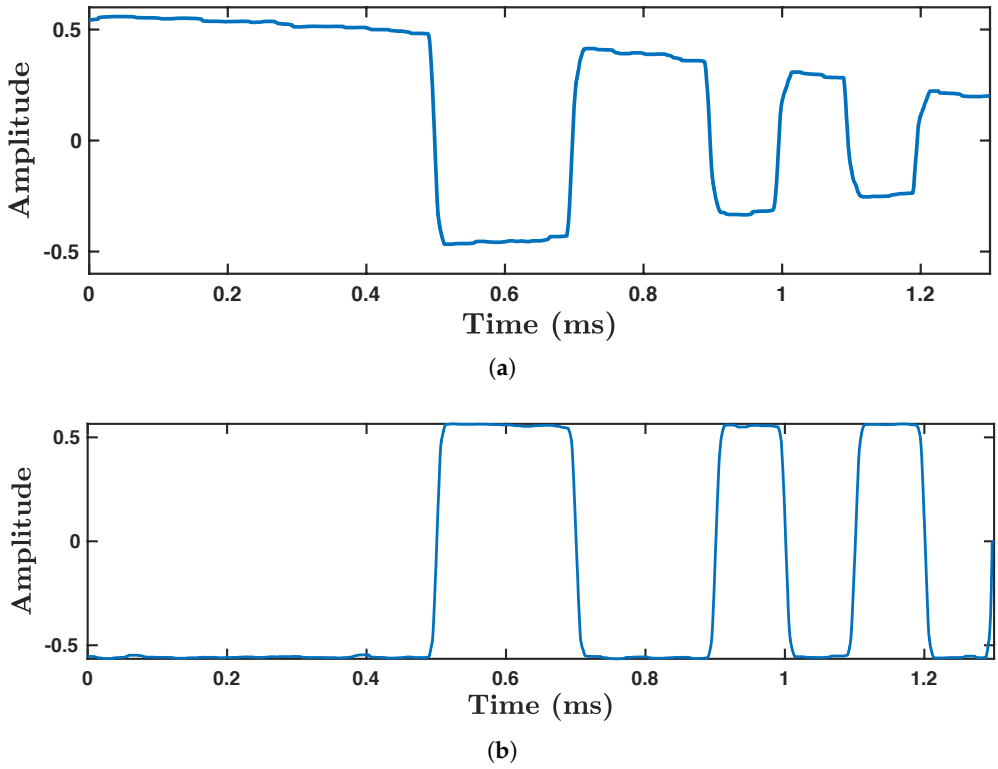


Figure 8. (**a**) Signal modulated with the Doppler residue. (**b**) Output of the proposed algorithm.

In the second iteration, $B(t)$ becomes the signal that is shown in Figure 8b. The new accumulated value of $\tilde{f}_d$ is 15.014 KHz, which is very close to the actual Doppler value of 15 KHz. In the third iteration, our local minmax detector did not find any local minima or maxima; therefore, it terminated the iterations and fed the estimated Doppler value to the block performing the waveform recovery and computing the target velocity.

The novelty of the proposed algorithm is that it converges in just a few iterations. In our case, it only took two iterations to achieve an accurate estimate of the Doppler value. Figure 9, the output of a Matlab workspace, concludes the above description.

```
Iteration No. 1

The estimated Doppler value of the itreration No. 1 = 14,822 Hz, with a difference 177 Hz
from actual value


Iteration No. 2

The estimated Doppler value of the itreration No. 2 = 15,014 Hz, with a difference 14 Hz
from actual value

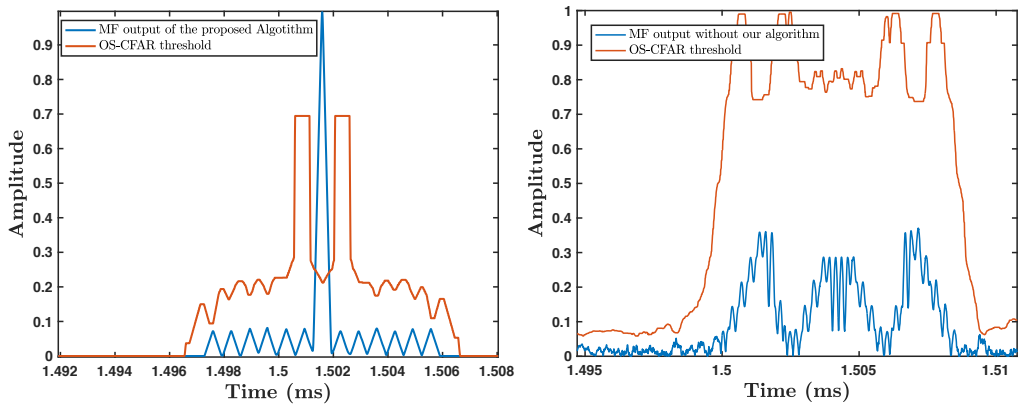


System does not need another iteration
>>
```

Figure 9. Matlab workspace for iterations of our proposed algorithm.

The MF output from the recovered waveform, compared to that of the conventional bi-phased pulse compression (PC) radar system, is shown in Figure 10. The output demon-

strates the superiority of our algorithm in estimating the exact Doppler value and perfectly recovering the signal compared to the conventional system.



(**a**) (**b**)

Figure 10. The MF output of a 15 KHz Doppler value (**a**) with the proposed algorithm and (**b**) without the proposed algorithm.

We evaluated the robustness of our new module by testing it at very low Doppler values, such as 150 Hz, and comparing it to the conventional PC radar system. The Matlab workspace results, shown in Figure 11, indicate that our module estimated the Doppler value to be 154 Hz, with a difference of just 4 Hz from the actual Doppler frequency.

```
Iteration No. 1

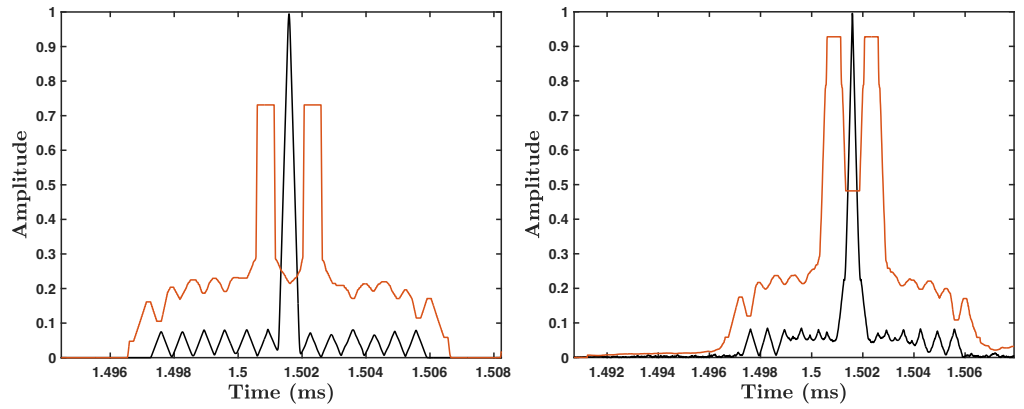
The estimated Doppler value of the itreration #1 = 154 Hz, with a difference 4 Hz from
actual value



System does not need another iteration
>>
```

Figure 11. Matlab workspace for iterations of our proposed algorithm to detect a 150 Hz Doppler value.

Although the conventional system was able to detect the target with a constant false alarm rate (CFAR), the signal was degraded both in the mainlobe and the near sidelobes, as shown in Figure 12b, compared to the MF output of our module depicted in Figure 12a.



(**a**) (**b**)

Figure 12. The MF output (in black) and the associated CFAR (in red) of a 150 Hz Doppler value (**a**) with the proposed algorithm and (**b**) without the proposed algorithm.

4. Performance Evaluation

To assess the performance of our proposed Doppler estimation and signal recovery system, two types of evaluations are discussed, namely, Doppler and detection evaluations. The first evaluation measures the SNR against different Doppler values, and the accuracy of the module is then calculated. The second evaluation measures the system SNR against the probability of detection. These evaluations offer a valuable understanding of how effective the proposed module is in practical and real-world applications.

Prior to evaluating our proposed algorithm, it is important to explain the reasoning behind categorizing Doppler values into low, medium, and high intervals, as well as the criteria used to select these intervals. Note that all calculations are performed in the S-band.

4.1. Selection Criteria for Doppler Value Intervals

The algorithm that we developed is capable of handling a wide range of Doppler values, from hundreds of Hz to several thousand Hz. We categorized these values based on the target speed as follows:

- Low-Doppler targets: This category includes various types of drones, such as consumer drones, racing drones, and some types of helicopters. Consumer drones typically have speeds ranging from 14 to 20 m/s, with advanced models reaching up to 30 m/s. Racing drones, designed for speed and agility, can exceed speeds of 45 m/s. Some types of helicopters, which are slower and used for specific tasks, also fall into this category. Consequently, the Doppler values for this category range from 100 Hz to 2000 Hz [21,22].
- Medium-Doppler targets: This category covers fixed-wing aircraft and commercial airplanes. Their average speeds range from 100 m/s to 350 m/s, resulting in Doppler values between 2000 Hz and 7000 Hz [22,23].
- High-Doppler targets: This category is dedicated to military aircraft, which have speeds ranging from 500 m/s to 750 m/s. The corresponding Doppler values for this category range from 10,000 Hz to 15,000 Hz [24].

To cover the full Doppler interval from 0 to 15 KHz, we choose the following Doppler ranges:

- Low-Doppler Range: 100–2000 Hz;
- Medium-Doppler Range: 2000–10,000 Hz;
- High-Doppler Range: 10,000–15,000 Hz.

4.2. Selected Threshold for Doppler Values

The Doppler value threshold should be selected such that the radar receiver can extract the target information without the need for our proposed algorithm. Therefore, if the proposed module is activated and the residue is less than the specific threshold, we can still obtain target information.

Based on the parameters listed in Table 1, the pulse width of the phase-coded waveform equals 1.3 ms. Hence, the Doppler completes one cycle during the pulse duration at 770 Hz. To avoid signal distortion, the Doppler value should be less than half of this value. To ensure good quality of the signal in the presence of the Doppler effect at the receiver end, the threshold is set to one-third of this value, approximately 256 Hz. Therefore, the Doppler value threshold is chosen to be 250 Hz.

4.3. Accuracy Evaluation

A cumulative distribution function (CDF) plot was selected to gain a deeper insight into the distribution of estimation errors across various Doppler values and SNR levels. Figure 13 shows the CDF plot of these estimation errors. The CDF was calculated based on randomly generated Doppler values from the low (100 Hz–2 kHz), medium (2–10 kHz),

and high (10–15 kHz) ranges, with SNRs spanning from −12 dB to 0 dB in 1 dB increments, and the calculations were repeated 1000 times each for a total of 39,000 trials.

A steeper slope in the CDF curve indicates more occurrences of smaller errors, particularly for values less than 100 Hz, with a 99.5% probability. This reflects the algorithm's ability to achieve precise Doppler estimation. Additionally, the plot reveals instances of larger errors occurring less frequently, with values of up to 1000 Hz having a 0.5% chance of occurring. This, however, can be addressed via an ensemble average over a few extra pulses.

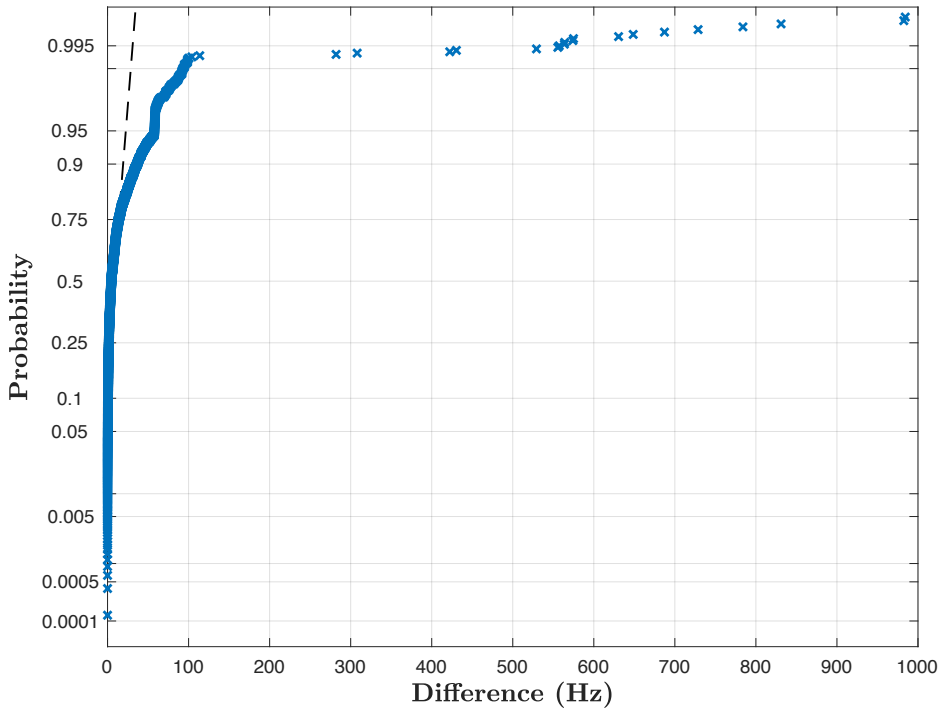


Figure 13. Cumulative probability of the estimation errors at different SNR values ranging from −12 dB to 0 dB with 1 dB increments. The dash line, representing the theoretical CDF of the normal distribution, is used as a reference.

To further gauge the accuracy of the proposed module, we rely on box plots. These plots allow us to examine the central tendency and spread of Doppler estimation errors at low, medium, and high Doppler values with a fixed SNR of −3 dB. In each case, the Doppler frequency to estimate is randomly selected and then tested 100 times. Figure 14 shows the results obtained. Remarkably, our algorithm consistently exhibited excellent performance across all three categories, with the absolute median estimation error not exceeding 30 Hz. It is important to note that the proposed algorithm has the ability to detect both positive and negative differences in all cases. The algorithm is designed to consistently check for these differences to prevent subtracting a value from a negative result, which could otherwise lead to an increase in the output error.

Table 2 provides a quantitative representation of the overall accuracy achieved by incorporating the proposed module into the radar system. The accuracy assessment was conducted based on the predetermined threshold value of 250 Hz (see Section 4.2), representing the maximum allowable frequency deviation to ensure the extraction of the main signal features without distortion. Additionally, the module was tested across a range of SNR values between −12 dB to 0 dB to provide a more comprehensive evaluation of the system's performance. The obtained results demonstrated notable accuracy levels, with a 100% accuracy rate being achieved at low Doppler values, 98.23% at medium Doppler values, and 96.32% at high Doppler values. These findings indicate the efficacy of the proposed module in maintaining high accuracy levels across a wide range of Doppler scenarios and SNR values, thereby validating its suitability for the intended application.

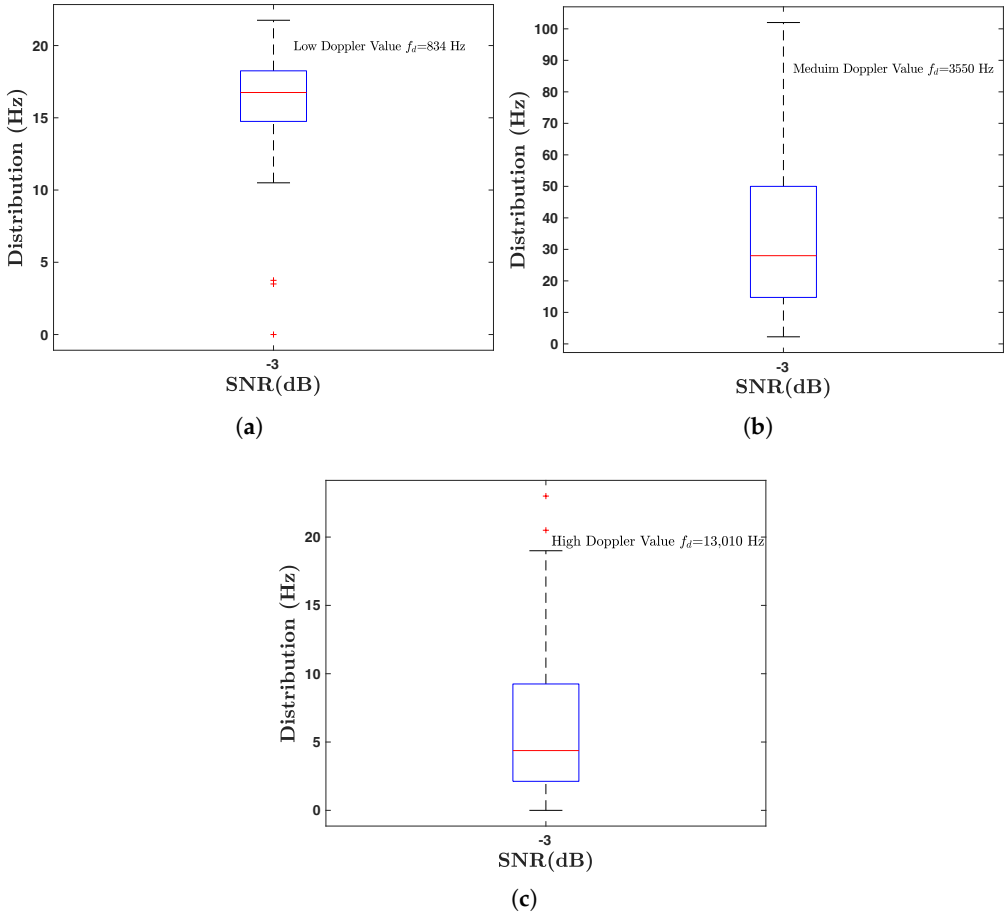


Figure 14. Box plot for the distribution of 100 trials on Doppler value data at SNR = −3 dB. (**a**) Low Doppler value of 834 Hz, (**b**) medium Doppler value of 2250 Hz, and (**c**) high Doppler value of 13,010 Hz.

Table 2. Average accuracy of the proposed algorithm.

Doppler Value	Average Accuracy	SNR Value
Low Value	100 %	−12:0 dB
Medium Value	98.2308%	
High Value	96.32%	

4.4. Probability of Detection Evaluation

The performance of the radar system with and without the proposed module is illustrated by the probability of detection (P_d) vs. SNR curves, which are depicted in Figure 15. To maintain a probability of false alarms (P_{fa}) of 10^{-6}, a typical value in radar systems, we used a CFAR processor. For each SNR value, we calculate the P_d value 500 times and plot the average. Doppler values from the low, medium, and high ranges were chosen to show the robustness of the proposed module. In fact, the module exhibited similarly excellent responses for all of these Doppler values. For an SNR greater than −12 dB, the three curves converge and practically achieve 100% detection. As the SNR decreases, the three curves diverge slightly, with medium and high Doppler values being better than the lower ones.

Comparing the detection curves of the proposed algorithm with the reference curve without the Doppler effect (indicated by the rhombus marker) reveals a degradation of 3 dB when compared to the medium-Doppler-value curve (indicated by the circle marker)

and 5 dB when compared to the low-Doppler-value curve (indicated by the cross marker). It is important to note that this degradation is considered acceptable when compared to the curve for which the Doppler effect (indicated by the pentagon marker) was applied but without using our module; the curve shows no detection at any given SNR values.

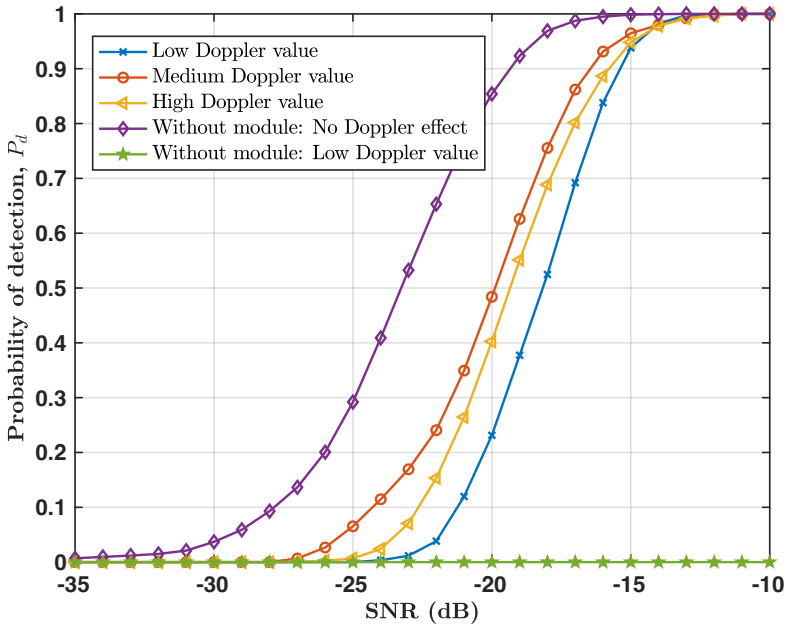


Figure 15. Probability of detection curve for the proposed algorithm with low (800 Hz), medium (3500 HZ), and high Doppler (13 KHz) values.

5. Proof of Concept

Traditional radar systems typically rely on dedicated hardware components for signal processing, waveform generation, and data analysis. However, by leveraging software-based processing in radar systems, such as in software-defined radar (SDR), multiple radar functions can be consolidated onto a single hardware platform, reducing equipment and maintenance costs [25–28]. This offers increased flexibility and adaptability, allowing for the rapid development and deployment of new radar functionalities. SDR platforms can be easily reprogrammed to support different radar modes, waveforms, and signal processing algorithms, enabling radar systems to be highly configurable [29–31].

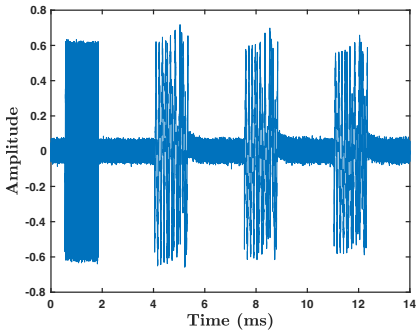
In this section, we present a proof of concept and a prototype for our proposed module in the radar system using SDR. The system uses two SDRs, one for transmitting the radar signal and holding the selected Doppler value and the other for receiving the transmitted signal. We also incorporated a synchronizer in our system by adding a marker signal, such as LFM or hyperbolic frequency modulation (HFM), to accurately estimate the beginning of the bi-phase signal at each CPI. We chose the LFM signal as our synchronizer because of its Doppler-tolerant nature. It is worth noting that we did not extract any information from the LFM signal; it was only used as a synchronization marker.

We provide the setup parameters of our experiment in Table 1, with the following adjustments based on the specifications of the SDRs used:

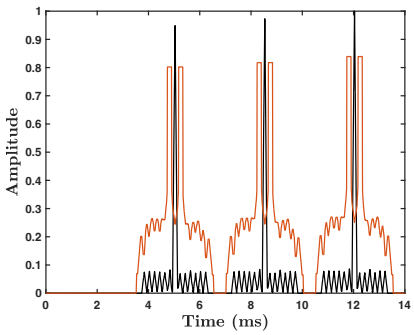
- SDR type: 2 USRPs N210;
- Sampling rate: 50 MHz;
- Band: 2.45 GHz—S-Band;
- Doppler values: 8, 10, and 15 KHz;
- LFM Bandwidth: 1 MHz.

We evaluated the performance of our module at the three different Doppler values of 8, 10, and 15 KHz, and we obtained the results shown in Figure 16. Note that we selected these specific values to test the system under challenging conditions within the medium- and

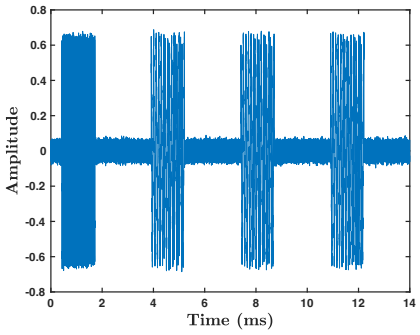
high-Doppler-frequency ranges. The results indicated that our module accurately estimated the Doppler values with minor differences from the actual values. More specifically, for the Doppler value of 8 KHz, the estimated value was 7.987 KHz, with a difference of only 12 Hz; for 10 KHz, the estimated value was 10.031 KHz, with a residue of 31 Hz; for 15 KHz, the estimate was 15.02 KHz, with a difference of 20 Hz. These results align with the simulation results recorded in Figure 13. Additionally, our module successfully recovered the well-known shape of the signal with all Doppler values, as observed in the MF output shown in Figure 16b,d,f. This result reflects the robustness and effectiveness of our proposed module in real-world applications, making it a valuable addition to any radar system.



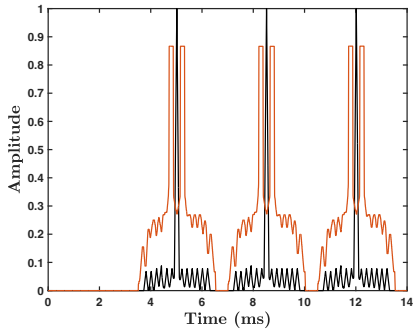
(**a**) Received signal with a Doppler value of 8 kHz.



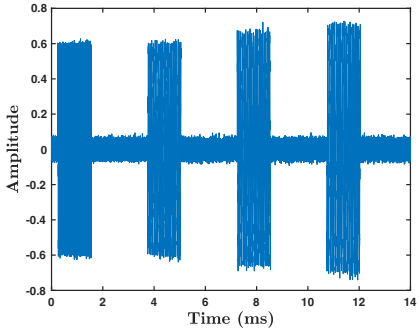
(**b**) MF output after removing the estimate Doppler value of 7.987 KHz.



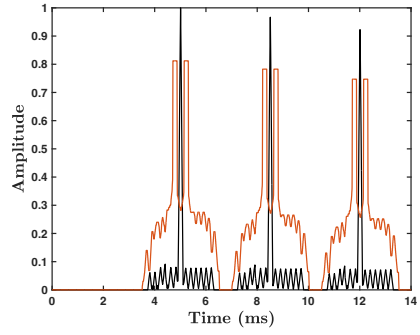
(**c**) Received signal with a Doppler value of 10 kHz.



(**d**) MF output after removing the estimate Doppler value of 10.031 KHz.



(**e**) Received signal with a Doppler value of 15 kHz.



(**f**) MF output after removing the estimate Doppler value of 15.02 KHz.

Figure 16. The received signal and MF output (in black) and the associated CFAR (in red) of the proposed module for different Doppler values. Top at 8 KHz, middle at 10 KHz, and bottom at 15 KHz.

6. Discussion

Although we have shown the effectiveness of integrating our proposed module into a radar system, it is crucial to acknowledge a few limitations and highlight several key points.

- While this paper primarily focuses on simulation results and a proof-of-concept implementation using SDR, experimental validation using real-world radar data presents practical difficulties due to the need for diverse targets, controlled conditions, and logistical considerations. Future research and collaboration with radar operators or institutions may be necessary to overcome these challenges and gather empirical evidence for the performance of the proposed module under real-world scenarios.
- The proposed module employs an iterative approach to estimate and correct the Doppler frequency. While iterations enhance accuracy, they can introduce computational complexity, potentially affecting real-time performance in practical applications. However, our simulation results showed that our module achieves efficient Doppler estimation with just one iteration at low and medium speeds and with two iterations at high and very high speeds, minimizing the computational burden while maintaining accurate results.
- The proposed module was specifically designed for signals with bi- and poly-phase modulation in mind, and it might require advanced nonlinear transformations for other modulation schemes. With that being said, by leveraging the capability of estimating the Doppler effect from a single pulse, a bi-phase signal can be used as a marker signal to compensate for the Doppler effect in other modulation schemes. This flexibility allows our algorithm to be used in MIMO systems, enabling accurate Doppler estimation and compensation across multiple antennas.
- Since there are no papers on radar systems that specifically address the estimation of the Doppler effect in the time domain and the subsequent recovery of the radar waveform, a direct comparison with other systems is not possible. Our proposed module fills this research gap by introducing a novel approach that enables Doppler estimation and radar waveform recovery. By leveraging this unique capability, our module offers distinct advantages in terms of accuracy and performance compared to existing methods in the literature.
- In practical scenarios, filtering is seldom perfect due to factors such as imperfect filter design, hardware limitations, environmental noise, and computational constraints. These non-ideal filtering conditions can introduce residual noise and interference into the signal, potentially affecting the performance of subsequent processing stages. In our experiments, we used two USRP SDR devices, one for transmission and the other for reception. Despite these non-ideal conditions, our results show that the system effectively handles such imperfections, maintaining robust performance and achieving promising results. Utilizing a software-defined platform allows for flexible adaptation to non-ideal filter conditions. This adaptability ensures that the system can be dynamically reconfigured to mitigate the effects of non-ideal filtering, thereby preserving the integrity of the signal-processing pipeline.
- The proposed radar system was not tested under jamming conditions, and it might experience degradation with some jamming techniques. It is important to note, however, that this degradation is not specific to our system alone; any radar system subjected to jamming attacks will inevitably experience performance degradation based on the jamming techniques employed. While recognizing the impact of jamming on radar systems, the primary focus of this paper is to present the novelty of the proposed module and its effectiveness in non-jammed scenarios. The investigation of the proposed module under jamming conditions has been deferred to a separate manuscript, as it requires a comprehensive analysis that would contribute valuable insights to the field of radar signal processing and anti-jamming techniques.

7. Conclusions

A novel and low-computational-complexity algorithm for Doppler estimation and signal recovery in bi-phase radar systems has been proposed. The algorithm is designed to accurately estimate the Doppler frequency and remove the Doppler effect from the received signal, allowing for precise range and velocity calculations.

The algorithm consists of several sub-modules, including a median filter, nonlinear transformation, local minmax detector, Doppler calculation module, Doppler checker, phase corrector, and bi-phase signal recovery. These sub-modules work together to iteratively estimate and reduce the Doppler effect from the received signal until the Doppler residue is zero or sufficiently small.

The excellent performance of the proposed system in estimating the Doppler effect and recovering the signal at different SNRs and Doppler values has been demonstrated. In addition, the implementation using SDR technology showed great potential.

Investigating the possibility of dynamically adapting the radar parameters, expanding the algorithm to handle scenarios with multiple targets simultaneously, and testing the algorithm under different background effects would be valuable extensions that will be the focus of our work in the near future.

Author Contributions: Conceptualization, A.Y. and B.M.; methodology, A.Y. and B.M.; software, A.Y.; validation, A.Y.; formal analysis, A.Y., B.M. and P.F.D.; investigation, A.Y., B.M. and P.F.D.; writing—original draft preparation, A.Y.; writing—review and editing, A.Y., B.M. and P.F.D.; visualization, A.Y., B.M. and P.F.D. All authors have read and agreed to the published version of the manuscript.

Funding: This research received no external funding.

Data Availability Statement: Data is contained within the article.

Acknowledgments: We would like to express our sincere gratitude to the anonymous reviewers for their valuable feedback and constructive comments, which greatly contributed to improving the quality of this paper. Their insightful suggestions were instrumental in shaping the final version of the manuscript. We would like to thank the Digital Research Alliance of Canada for their valuable computational resources and services.

Conflicts of Interest: The authors declare no conflict of interest.

References

1. Richards, M.A.; Holm, W.A. *Principles of Modern Radar: Basic Principles*, 2nd ed.; IET Radar, Sonar and Navigation Series; Scitech Publishing: London, UK, 2023.
2. Mahafza, B.R. *Radar Systems Analysis and Design Using MATLAB*, 4th ed.; CRC Press Chapman & Hall: Boca Raton, FL, USA, 2022.
3. Cook, C. *Radar Signals: An Introduction to Theory and Application*; Elsevier: Amsterdam, The Netherlands, 2012.
4. Levanon, N.; Mozeson, E. *Radar Signals*; John Wiley & Sons: Hoboken, NJ, USA, 2004.
5. Alaee-Kerahroodi, M.; Babu, P.; Soltanalian, M.; Shankar, M.R.B. *Signal Design for Modern Radar Systems*; Artech House: Norwood, MA, USA, 2022.
6. Budge, S.R.G.O. *Basic Radar Analysis*, 2nd ed.; Artech House: Norwood, MA, USA, 2020.
7. Peng, Z.; Li, C.; Uysal, F. *Modern Radar for Automotive Applications*; IET Radar, Sonar and Navigation Series; The Institution of Engineering and Technology: Hertfordshire, UK, 2022.
8. Jian Wang, J.L. *Motion and Gesture Sensing with Radar*; Artech House Radar Library, Artech House: Norwood, MA, USA, 2022.
9. Hwang, C.H.; Kim, K.M.; Chun, S.Y.; Lee, S.K. Doppler Estimation Based on Frequency Average and Remodulation for Underwater Acoustic Communication. *Int. J. Distrib. Sens. Netw.* **2015**, *2015*, 746919. [CrossRef]
10. Ferdman, Y.; Yekutieli, D.; Sochen, N. A method for radar detection and range-Doppler estimation. In Proceedings of the 2017 IEEE International Conference on Microwaves, Antennas, Communications and Electronic Systems (COMCAS), Tel-Aviv, Israel, 13–15 November 2017; pp. 1–6.
11. Xin, M.; Li, W.; Wang, X.; Zhang, Y.; Xu, L. Preamble Design with HFMs for Underwater Acoustic Communications. In Proceedings of the 2018 OCEANS—MTS/IEEE Kobe Techno-Oceans (OTO), Kobe, Japan, 28–31 May 2018; pp. 1–5.
12. Li, W.; Ren, L.; Mao, E.; Fan, H. Doppler compensation method for the complementary phase-coded signal. *J. Eng.* **2019**, *2019*, 7521–7524. [CrossRef]
13. Wei, R.; Ma, X.; Zhao, S.; Yan, S. Doppler Estimation Based on Dual-HFM Signal and Speed Spectrum Scanning. *IEEE Signal Process. Lett.* **2020**, *27*, 1740–1744. [CrossRef]

14. Lin, X.; Lin, Z.; Löwenmark, S.E.; Rune, J.; Karlsson, R. Doppler Shift Estimation in 5G New Radio Non-Terrestrial Networks. *arXiv* **2021**, arXiv:2108.07757. [CrossRef]
15. Youssef, A.; Driessen, P.F.; Gebali, F.; Moa, B. A Novel Framework for Combining Multiple Radar Waveforms Using Time Compression Overlap-Add. *IEEE Trans. Signal Process.* **2021**, *69*, 4371–4384. [CrossRef]
16. Zhang, J.; Su, T. High-speed maneuvering target detection and motion parameter estimation. In Proceedings of the 2016 CIE International Conference on Radar (RADAR), Guangzhou, China, 10–13 October 2016; pp. 1–4. [CrossRef]
17. Zahra, A.G.; Mehany, W.; Ahmed, F.M.; Youssef, A. Radar detection and speed estimation of high-speed targets using phase-modulated waveforms. *Electron. Lett.* **2023**, *59*, e12918. [CrossRef]
18. Huang, T.; Yang, G.; Tang, G. A fast two-dimensional median filtering algorithm. *IEEE Trans. Acoust. Speech Signal Process.* **1979**, *27*, 13–18. [CrossRef]
19. Storath, M.; Weinmann, A. Fast Median Filtering for Phase or Orientation Data. *IEEE Trans. Pattern Anal. Mach. Intell.* **2018**, *40*, 639–652. [CrossRef] [PubMed]
20. Lindsey, W.; Simon, M. Carrier Synchronization and Detection of Polyphase Signals. *IEEE Trans. Commun.* **1972**, *20*, 441–454. [CrossRef]
21. Flying-a-Drone-at-High-Speed. 2024. Available online: https://www.autelpilot.com/blogs/news/flying-a-drone-at-high-speed (accessed on 11 June 2024).
22. How-Fast-Do-Helicopters-Fly. 2024. Available online: https://pilotinstitute.com/how-fast-do-helicopters-fly/ (accessed on 11 June 2024).
23. Commercial-Planes-Fly-Guide. 2024. Available online: https://aviex.goflexair.com/flight-school-training-faq/commercial-plane-speeds (accessed on 11 June 2024).
24. Fastest-Fighter-Jets-Guide. 2024. Available online: https://simpleflying.com/fastest-fighter-jets-guide/ (accessed on 11 June 2024).
25. Collins, T.F.; Getz, R.; Pu, D.; Wyglinski, A.M. *Software-Defined Radio for Engineers*; Artech House Mobile Communications Series; Artech House Publishers: Norwood, MA, USA, 2018.
26. Crockett, L.; David Northcote, R.W.S. *Software Defined Radio with Zynq UltraScale+ RFSoC*, 1st ed.; Strathclyde Academic Media: Glasgow, UK, 2023.
27. Laufer, C. *The Hobbyist's Guide to the RTL-SDR: Really Cheap Software Defined Radio: A Guide to the RTL-SDR and Cheap Software Defined Radio by the Authors of the RTL-SDR.com Blog*, 4th ed.; CreateSpace Independent Publishing Platform: Scotts Valley, CA, USA, 2015.
28. Donat, W. *Explore Software Defined Radio: Use SDR to Receive Satellite Images and Space Signals*, 1st ed.; Pragmatic Bookshelf: Raleigh, NC, USA, 2021.
29. Hershberger, J.; Pratt, T.; Kossler, R. Implementations of Coherent Software-Defined Dual-Polarized Radars. *IEEE Trans. Microw. Theory Tech.* **2017**, *65*, 1673–1681. [CrossRef]
30. Tuysuz, B.; Urbina, J.; Lind, F.D. Development of a passive VHF radar system using software-defined radio for equatorial plasma instability studies. *Radio Sci.* **2013**, *48*, 416–426. [CrossRef]
31. Vargas, A.; Lvarez, R.; Lupera, P.; Grijalva, F. SDR-based Speed Measurement with Continuous-Wave Doppler Radar. In Proceedings of the 2021 IEEE International Mediterranean Conference on Communications and Networking (MeditCom), Athens, Greece, 7–10 September 2021; pp. 401–406.

Disclaimer/Publisher's Note: The statements, opinions and data contained in all publications are solely those of the individual author(s) and contributor(s) and not of MDPI and/or the editor(s). MDPI and/or the editor(s) disclaim responsibility for any injury to people or property resulting from any ideas, methods, instructions or products referred to in the content.